ELSEVIER

Physica C 252 (1995) 125–137

PHYSICA C

Growth-induced columnar defects in $YBa_2Cu_3O_{7-x}$ thin films grown on miscut mosaic $LaAlO_3$ (001)

Z.L. Wang [a], D.H. Lowndes [b], D.K. Christen [b], D.M. Kroeger [c], C.E. Klabunde [b], D.P. Norton [b]

[a] *School of Materials Science and Engineering, Georgia Institute of Technology, Atlanta, GA 30332-0245, USA*
[b] *Solid State Division, Oak Ridge National Laboratory, Oak Ridge, TN 37831, USA*
[c] *Metals and Ceramics Division, Oak Ridge National Laboratory, Oak Ridge, TN 37831, USA*

Received 19 June 1995

Abstract

Measurements of the critical current density in $YBa_2Cu_3O_{7-x}$ (YBCO) thin films grown on deliberately miscut (1.6°) $LaAlO_3$ {001} substrates that also contain a small mosaic spread of subgrain orientations have shown an anomalous angular dependence of J_c. A strong, magnetic field-dependent peak in J_c is observed when the magnetic field is oriented between the *c*-axis (the film normal direction) and the *a*–*b*-plane; in this orientation flux pinning is normally not strong. Transmission electron microscopy (TEM) has been used to determine the defects which are responsible for the flux pinning related to the anomalous J_c peak. [001] columnar defects have been observed to penetrate right through the YBCO films. The diameters of the columnar defect regions are ~ 3–5 nm, which is near ideal for producing the observed anomalous pinning and high J_c. Numerous stacking faults involving excess Cu–O layers have also been observed; these can also serve as effective flux pinners. Small-angle planar boundaries perpendicular to the substrate are rarely seen. Images of the YBCO–substrate interface reveal that some of the columnar growth defects initiate at substrate steps/dislocations. The YBCO unit cells grown on the upper and lower terraces of a substrate step have a relative shift of $c/3$[001]; thus, the Cu–O planes are broken within a region less than 10 nm from the substrate, presumably reducing the superconducting order parameter in this region and leading to pinned vortices situated on these sites. Thus, the columnar defects initiated from the interface and the stacking faults are useful for pinning flux through the entire film thickness.

1. Introduction

In epitaxial crystal growth, the substrate should meet several specifications in order to grow high-quality films. The lattice constant of the substrate should be closely matched to that of the film, so that the density of interfacial dislocations is minimized. The substrate should not have phase transformations at the growth temperature of the film. Only a minimal chemical reaction can be tolerated in the interface regions between the substrate and the film. In epitaxial growth of high-temperature superconducting thin films, lanthanum aluminate ($LaAlO_3$) is one of the optimum substrate candidates [1,2]. $LaAlO_3$ has the distorted-perovskite structure with lattice constant $a = b = c = 0.3788$ nm and $\alpha = \beta = \gamma = 90.066°$ [3,4]. The small (< 2%) lattice mismatch between $LaAlO_3$ and $YBa_2Cu_3O_{7-x}$ allows high quality *c*-axis oriented superconducting thin films to be grown on the (100) surface.

For high-temperature superconductors the introduction of defects with appropriate size, shape, and

SSDI 0921-4534(95)00428-9

density can greatly enhance the critical current density. For example, columnar defects have been produced by several groups using heavy-ion irradiation. Lowndes et al. [5] recently reported a technique in which effective flux-pinning defects were created during film growth, by growing $YBa_2Cu_3O_{7-x}$ (YBCO) thin films on deliberately miscut (1.6°) $LaAlO_3$ {001} (LAO) substrates that also contained a small mosaic spread of subgrain orientations. The normal direction of the substrate surface slightly deviates from that of the (001) crystallographic plane, resulting in many steps on the substrate surface and leading to the growth-induced defects. Measurements of critical current density in miscut-grown YBCO thin films have shown an anomalous angular dependence of J_c. A strong, magnetic field-dependent peak in J_c is observed when the magnetic field is oriented between the c-axis (the film normal direction) and the CuO_2 plane (or a–b-plane), an orientation where flux-pinning is not normally strong. Preliminary transmission electron microscopy (TEM) observations revealed columnar defects of diameters ~ 3–5 nm that are aligned nearly parallel to the c-axis [6]. This array of defects may be responsible for the strong flux pinning and high J_c.

In this paper, high-resolution transmission electron microscopy (HRTEM) is applied to extensively study the defect structures formed in the YBCO films grown on the miscut and slightly mosaic $LaAlO_3$ {001} substrates. The nature of the defects as well as small-angle planar boundaries are examined from both cross-section and planar-view TEM specimens. The interface between the film and the substrate has also been examined, with the result that the substrate steps/dislocations are shown to be the favored sites for growing the columnar defects. It is also shown that the substrate steps/dislocations are responsible for the growth of many types of defects, which also should be effective flux pinners for the entire film thickness. Therefore, it appears that proper control of the density of steps and dislocations on the substrate surface can greatly affect the critical current density of the entire film.

2. Anomalous flux-pinning phenomenon

The YBCO films of thickness ~0.5 μm were grown by pulsed KrF laser ablation on miscut $LaAlO_3$ {001} substrates using standard procedures for pulsed laser ablation film growth that have been described elsewhere [7]. The magnetic field dependence and the field angular dependence of J_c were measured before the TEM experiments. Fig. 1 shows the experimentally measured critical current density $J_c(H, \theta)$ as a function of the applied magnetic field strength, H, and the angle between H and the c-axis [5]. The anisotropy of $J_c(H, \theta)$ is strongly modified, in comparison to that of a film on accurately cut $SrTiO_3$. Although the highest J_c still occurs for H parallel to the Cu–O planes [the a–b-plane], the minimum J_c points are no longer at $H \| c$ symmetrically between the two J_c peaks, and a large new asymmetrically positioned J_c peak appears. It is apparent that the anomalous peak in J_c shifts toward the c-axis with increased H. The peak reaches a maximum, relative to the intrinsic pinning, for $H = 0.5$ T, and then decreases more rapidly than does the intrinsic pinning for $H > 1$ T. The strength and angular dependence of the anomalous flux pinning suggests that the flux lines in YBCO are pinned over an appreciable fraction of their length, i.e. oriented, extended defects are expected.

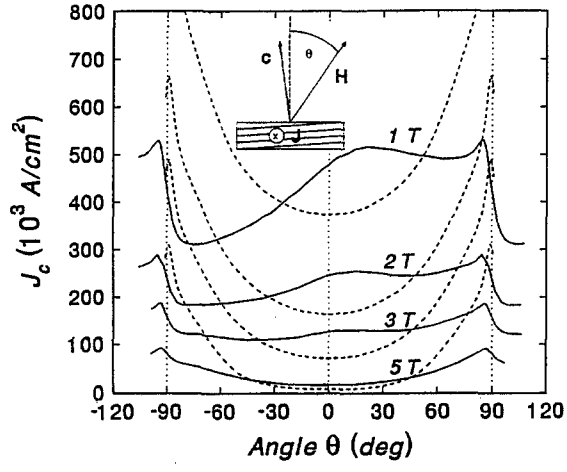

Fig. 1. J_c(H, θ) at T = 77 K and H = 1, 2, 3 and 5 T, for epitaxial YBCO films grown (solid curves) on $LaAlO_3$ miscut ~ 1.6° away from (001) and (dashed lines) on accurately cut (001) $SrTiO_3$. The angular shift of the YBCO/$LaAlO_3$ data by the ~ 1.6° miscut angle is apparent, as are the angle-asymmetric enhancements in J_c for field orientations near the c-axis. The intrinsic pinning peaks at $H \| a$–b are reduced due to the miscut, perhaps because of defect-induced misorientations of the lattice planes.

The objective of this study is to identify the flux-pinning sites which are responsible for the newly observed J_c. Cross-sectional and planar-view TEM specimens were prepared in order to examine the microstructure of the film–substrate interface and the defects initiated from the interface. HRTEM studies were performed using a Philips CM30 TEM (300 kV) and a Hitachi HF-2000 TEM (200 kV).

3. Effective flux-pinners

3.1. TEM of cross-section specimens

Fig. 2 shows a low-magnification cross-section TEM image of a *c*-axis-oriented YBCO thin film grown on the (001) surface of $LaAlO_3$. The electron diffraction pattern recorded from the cross-section TEM specimen, shown in the inset of Fig. 2, exhibits an epitaxial relationship between the YBCO film and the substrate,

$$(001)_{YBCO} \| (001)_{LAO} \quad \text{and} \quad [100]_{YBCO} \| [100]_{LAO}.$$

The YBCO film is single crystalline and the growth direction is [001]. No apparent interface reaction is seen. More importantly, columnar defects are formed in the film and grow from the film–substrate interface through the entire film thickness. The columnar defects are oriented near the *c*-axis (nearly perpendicular to the substrate surface), thus accounting for the observed anomalous pinning and high J_c with a magnetic field oriented in non-symmetry directions

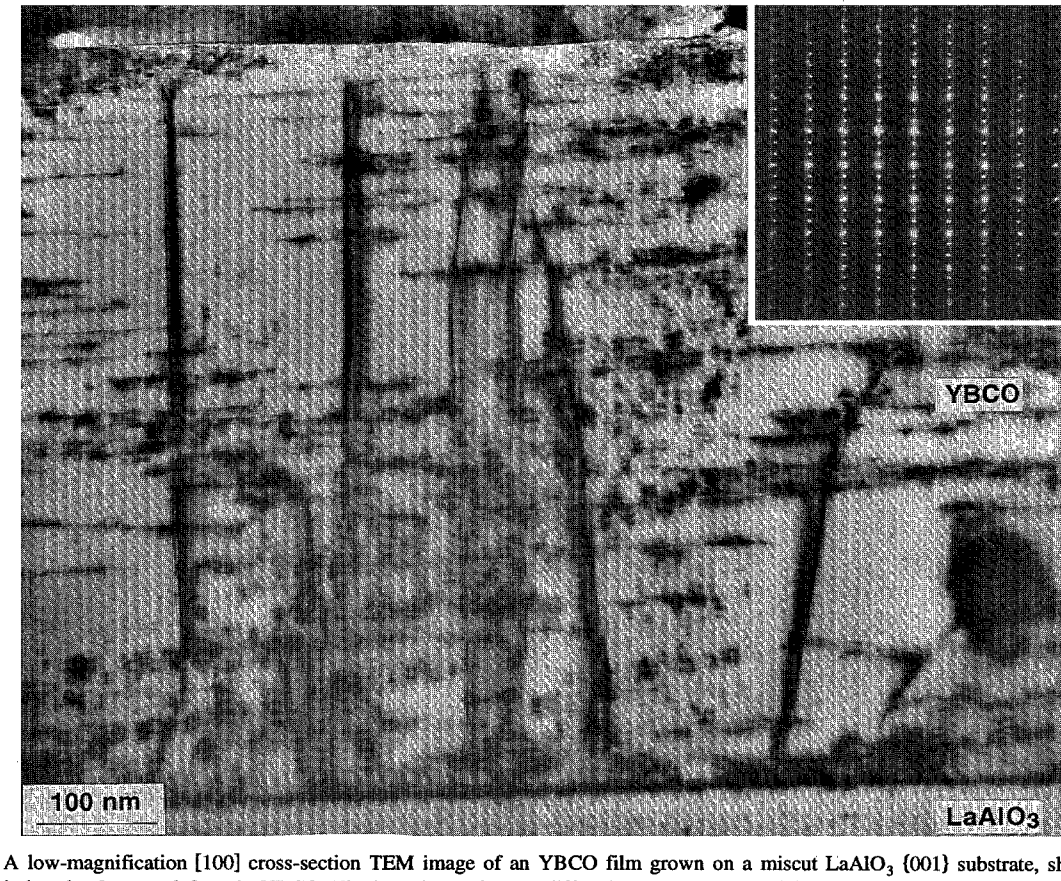

Fig. 2. A low-magnification [100] cross-section TEM image of an YBCO film grown on a miscut $LaAlO_3$ {001} substrate, showing the growth-induced columnar defects in YBCO. The inset is an electron diffraction pattern recorded from this region.

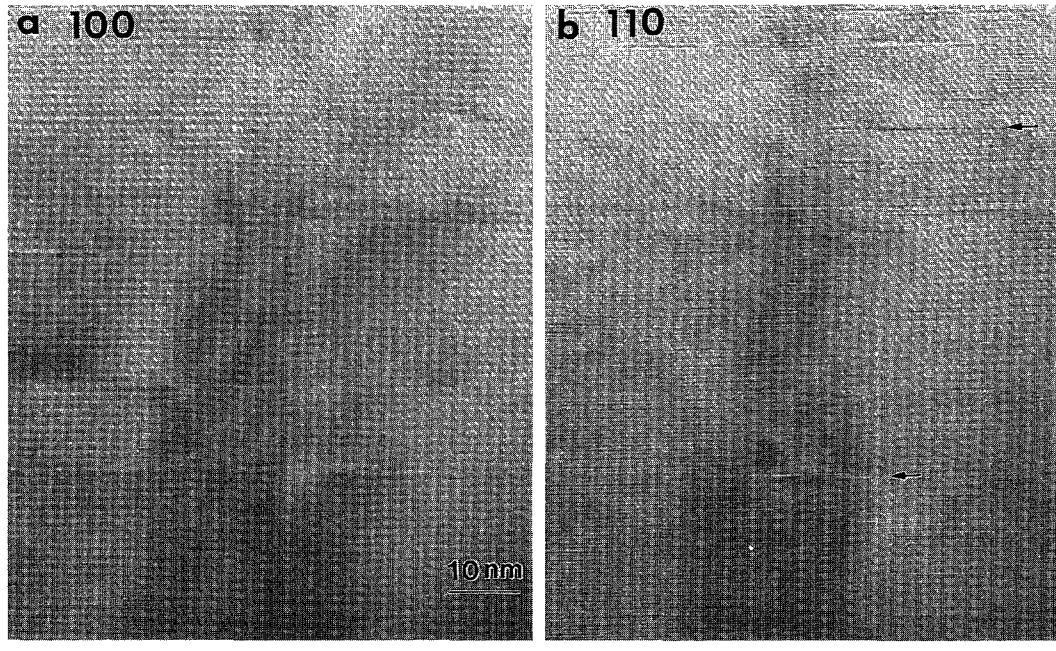

Fig. 3. High-magnification [100] cross-section TEM images of YBCO film when the incident beam direction is (a) [100] and (b) [110], showing the formation of a [001] columnar defect. The arrowheads indicate small size stacking faults lying in the (001) plane.

near the c-axis of the $YBa_2Cu_3O_{7-x}$ film [4,11]. In addition, numerous small stacking faults lying in the a–b-plane are also produced by the columnar defects. These faults can also be effective flux pinners [8].

To verify whether the defects observed in Fig. 2

Fig. 4. A dark-field, weak-beam cross-section image of a YBCO film showing columnar defects initiated from the substrate surface.

are columnar defects, the specimen was rotated from [100] orientation to [110] orientation around the c-axis (or [001]) of YBCO. The width of the defect would broaden if it was a planar defect. Figs. 3(a) and (b) show two images of the same defect before and after the specimen was rotated by 45° around [001]. The effective width of the defect was unchanged, indicating its columnar nature. In general, the contrast width measured from a TEM image of a columnar defect is larger than the actual structural width of the defect owing to the long-range diffraction contrast produced by the residual strain from the defect. Based on the observation of the columnar defect in Fig. 3, the structural width of the defect is approximately 3–5 nm, which is comparable to the vortex core diameter in YBCO and is therefore ideally suited for pinning flux when the magnetic field is parallel to the c-axis [9].

Most of the dislocations initiated from the YBCO–substrate interface are columnar defects. This result is obtained from dark-field, weak-beam images of the YBCO cross-section, as shown in Fig. 4. Weak-beam imaging is a technique that is most suited for imaging defects in crystalline specimens,

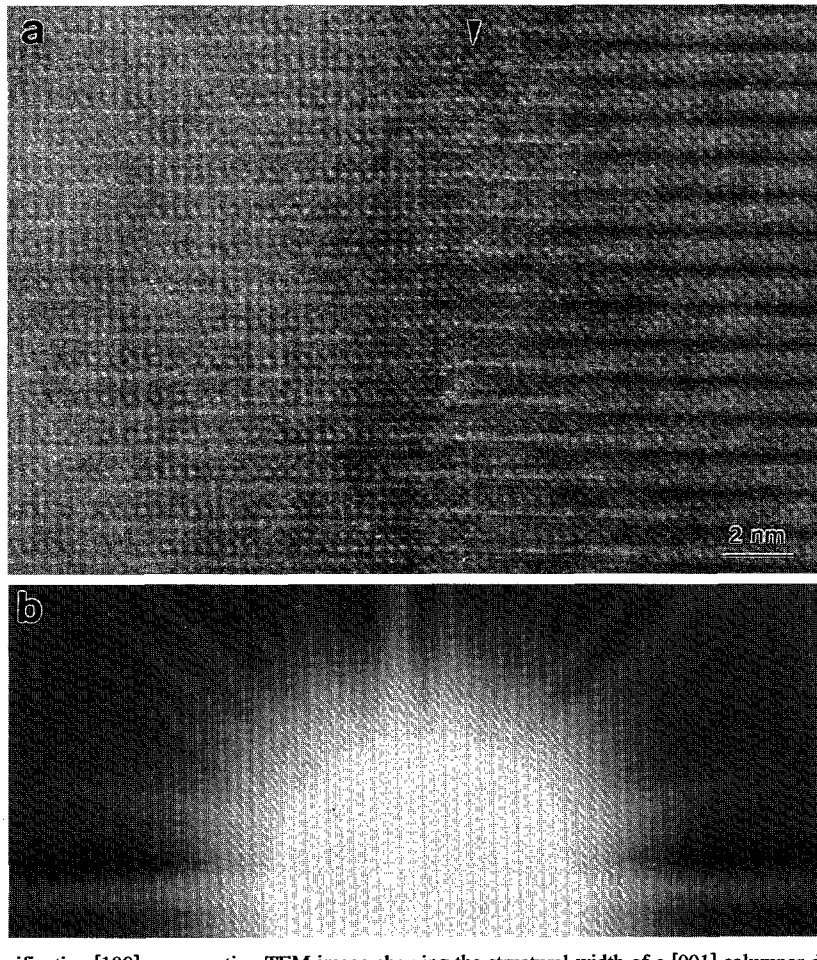

Fig. 5. (a) A high-magnification [100] cross-section TEM image showing the structural width of a [001] columnar defect. (b) A convergent beam Kikuchi pattern recorded from the defect region showing a small lattice rotation around [001].

particularly for defects distributed at grain boundaries and interfaces. Under the "two-beam" Bragg diffracting condition far from either [100] or [110] zone axis, the image is recorded using a weakly diffracted beam. The (110) twin planes are visible in the image. The defects show line-type contrast, indicating columnar character. Some of the defect lines are parallel to [001] and penetrate through the entire film thickness. Some of the defects are curved. The curved defects tend to terminate inside the YBCO film. However, a common feature is that all the defects are initiated from the YBCO–substrate interface, indicating the importance of the substrate microstructure for the growth of YBCO films.

The YBCO lattice around a columnar defect is slightly distorted, resulting in a small rotation of the crystal lattice on both sides of the defect. An HRTEM image recorded from a columnar defect, as shown in Fig. 5(a), reflects the slight tilt of the crystal across the defect. The Cu–O planes or layers remain continuous; thus, the superconductivity should be preserved. The structural width of the defect is less than 2 nm, ideal for *c*-axis flux pinning. A convergent beam Kikuchi pattern [Fig. 5(b)] recorded from the region shows the relative rotation of the crystal about [001]. The rotation angle can be directly measured from the Kikuchi pattern and is approximately 0.6°.

Although the observed defects are mostly columnar, small-angle planar boundaries are also observed. Figs. 6(a) and (b) show two TEM images of the same specimen region before and after 45° rotation around [001]. It is apparent that the width of the defect is significantly broadened after being rotated from [100] to [110]. Thus, the defect is a (010) planar defect. Planar defects are also expected to pin flux but they may not be as effective as the columnar

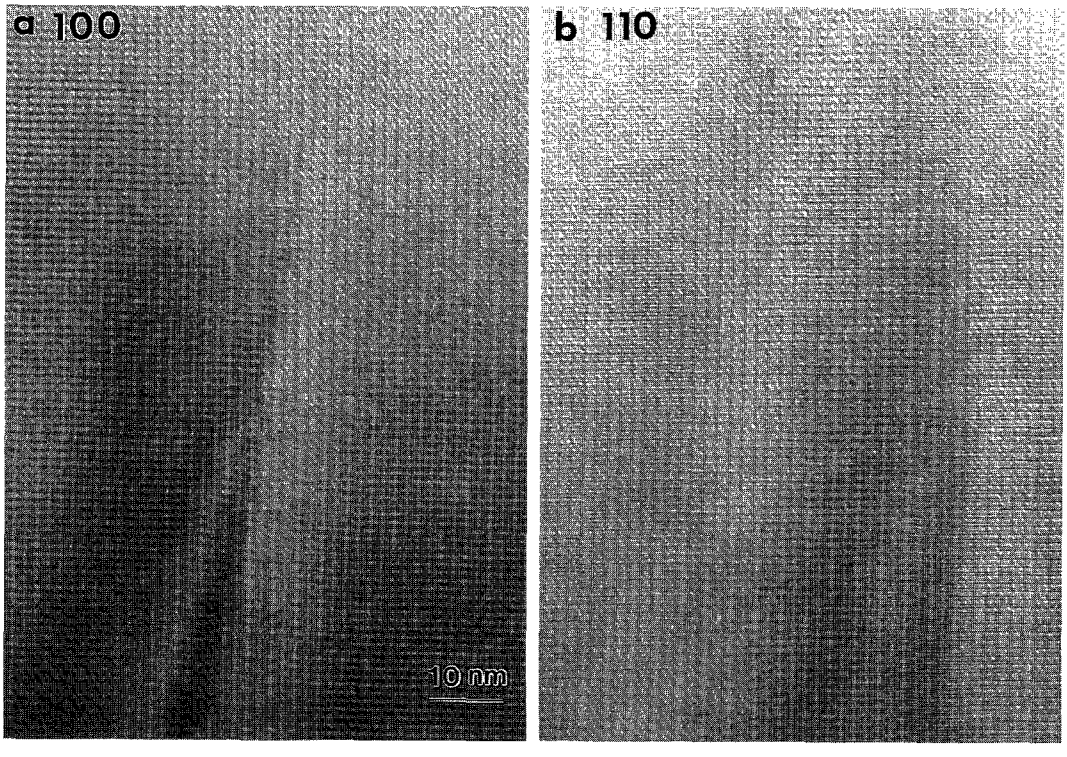

Fig. 6. High-magnification [100] cross-section TEM images of a YBCO film when the incident beam direction is (a) [100] and (b) [110], showing the presence of a small-angle boundary. The boundary plane is nearly parallel to (010).

defects because their pinning efficiency depends on the direction of the current-induced vortex driving force; vortex motion within a plane is not effectively inhibited.

In addition to the columnar defects, stacking faults have been observed. The stacking faults lie in the (001) plane with diameters of a few to a few tens of nm. To find the nature of the stacking faults in this case, HRTEM images were recorded when the incident beam was parallel to [100]/[010], as shown in Fig. 7. In reference to the previous image simulation [10], it is apparent that the stacking faults are produced by excess Cu–O layers in the (001) plane. The density of stacking faults is higher near the columnar defects, suggesting that the stacking faults are created in order to compensate the strains produced from the columnar defects, similar to the high density of stacking faults observed near Y_2BaCuO_y particles in melt-textured YBCO [8].

3.2. TEM of planar-view specimens

To confirm the results observed in cross-section specimens, planar-view TEM specimens were prepared. Fig. 8 shows a TEM image of the YBCO film when the incident beam direction is near [001]. From the electron diffraction pattern, shown in the inset of Fig. 8, the entire film is single crystalline. However, the bright-field image shows strong diffraction contrast due to lattice distortion by the high-density a–b-plane stacking faults, [001] columnar defects and the defects initiated from the substrate surface within 10 nm from the substrate. At low magnification, the columnar defects along [001] are densely distributed so that the features of each individual defect cannot be clearly resolved. A low-angle boundary is seen in Fig. 8, but there is almost no relative rotation between the two "grains" of the boundary, in agreement with the observation shown in Fig. 5.

Fig. 9 shows a high-magnification [001] lattice image of YBCO. A columnar defect of diameter about 5–7 nm is observed. The thickness of the specimen at this region is approximately 100 nm; thus, the lattice image contrast is greatly reduced at the region containing the defect, due to projection effect. This image is consistent with the observations made from cross-section specimens.

Small-angle boundaries also are observed in the planar-view specimens, as shown in Fig. 10. The grain boundary angle is so small that it is hardly measurable from the electron diffraction pattern. The HRTEM image clearly shows the planar boundaries, as indicated by arrowheads. However, the density of columnar defects is much higher than the density of planar boundaries. Therefore, the flux-pinning from columnar defects is dominant.

4. YBCO–substrate interface

As shown in Fig. 2, images of the YBCO–substrate interface revealed that almost all the columnar defects are initiated at the substrate surface. Consequently, it is necessary to examine the interface structure at high magnification. Fig. 11 shows a cross-section HRTEM image of the YBCO-substrate interface. A columnar defect apparently is initiated at a substrate step, as indicated by an arrowhead. In this case, the columnar defect does not penetrate through the thickness of the entire film; instead it ends at the eighth unit cell. The YBCO unit cells grown on the upper and lower terraces of the substrate step are shifted by $c/3$[001], so that the Cu–O chains are broken, possibly resulting in the decrease or disappearance of superconductivity locally. The Cu–O

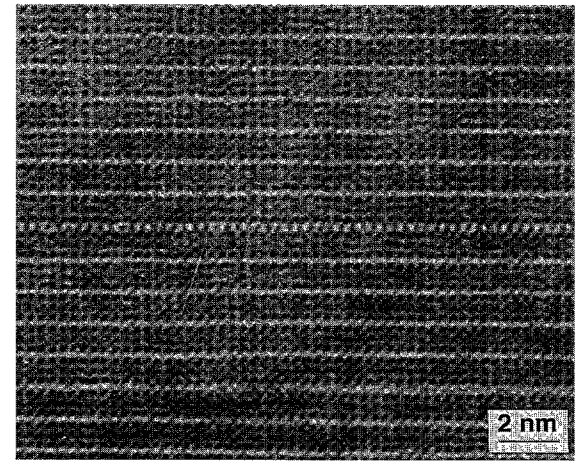

Fig. 7. A high-magnification [100] cross-section TEM image of YBCO showing a stacking fault produced by an excess Cu–O layer.

chains on both sides of the defect are re-matched due to the creation of stacking faults with excess Cu–O layers, as indicated in Fig. 11. Thus, a strong strain field is expected within the first few YBCO unit cells. The termination of the columnar defects within the YBCO film is consistent with the result shown in the dark-field, weak-beam image in Fig. 4. This suggests that proper control of the density of the surface steps/dislocations may affect the density of columnar defects, possible resulting in a further increase of the critical current density when the magnetic field direction is between the *c*-axis and the *a*–*b*-plane of YBCO. However, increasing the substrate miscut angle to only $\sim 6°$ can actually decrease the low-field J_c of nominally *c*-axis perpendicular YBCO films [5].

Fig. 12 shows another case of two columnar defects initiated from the substrate surface. The de-

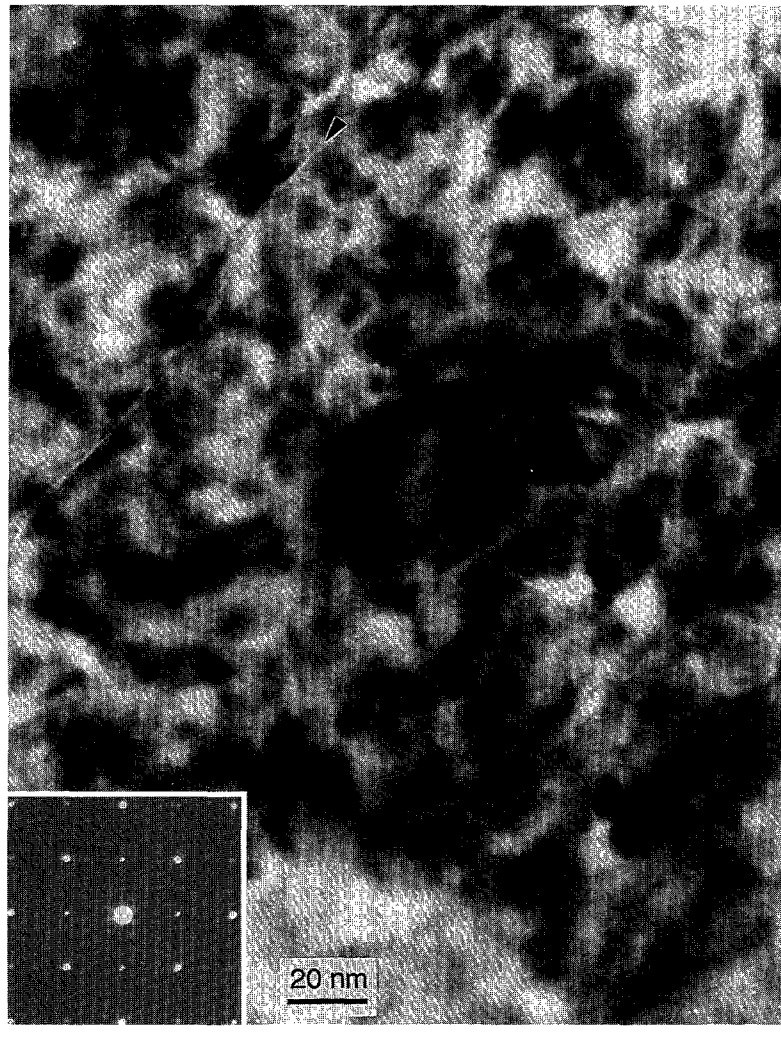

Fig. 8. A low-magnification [001] planar-view TEM image of a YBCO film showing strong diffraction contrast due to columnar defects and stacking faults. The inset is an electron diffraction pattern recorded from this region.

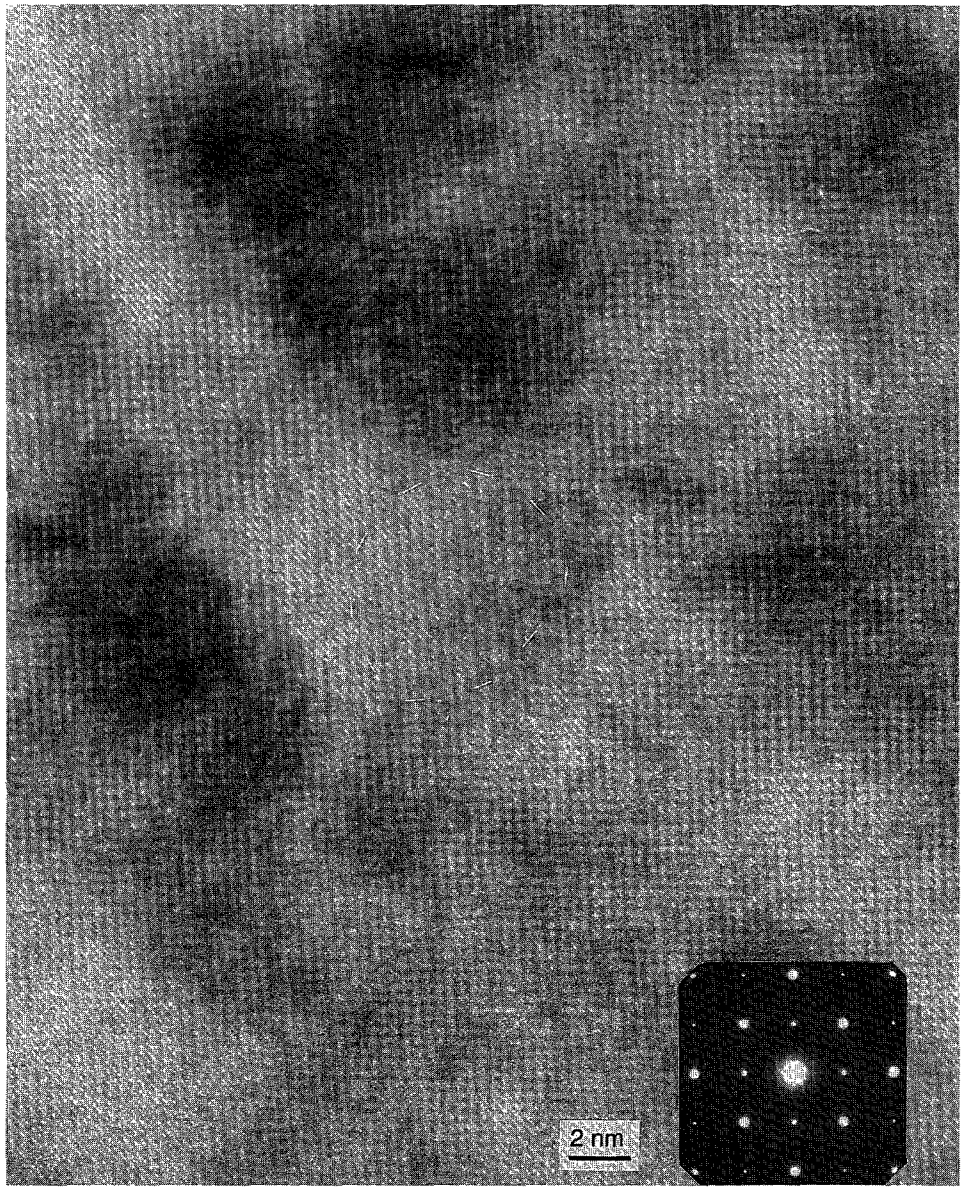

Fig. 9. A high-magnification [001] planar-view TEM image of YBCO showing a [001] columnar defect. The inset is an electron diffraction pattern recorded from this region.

fects end at the seventh YBCO unit cell due to the creation of stacking faults. For the YBCO material more than about 10 nm away from the substrate surface, the Cu–O planes are continuous. For these defects, only a small fraction of the vortex length would be pinned effectively. It is unlikely that these

defects play a dominant role in enhancing J_c, but rather the long columns as shown in Fig. 2.

5. Discussion

Columnar defects initiated at the surface growth steps and mosaic-induced dislocations of nominal (100), miscut $LaAlO_3$ substrates penetrate through the grown YBCO films and are aligned near the c-axis. Since the diameters of the defective regions are ~ 3–5 nm (Fig. 2), these defects are ideal for pinning vortices in YBCO for which the vortex core diameter is ~ 3 nm. Maximum flux pinning due to the columnar defects alone is expected when the applied magnetic field H is aligned nearly parallel to the defect columns, i.e., near the c-axis which normally is a low-J_c orientation in c-axis perpendicular YBCO films. Consequently, in YBCO films grown on miscut $LaAlO_3$ substrates that also contain some mosaic spread of substrate grain orientations, a new J_c peak appears between the c-axis and the a–b planes, as shown in Fig. 1.

The columnar defects are analogous to the continuous non-superconducting tracks produced by heavy-ion irradiation [12,13]. From the micrographs, the density of the columnar defects in the present specimens appears sufficient to pin nearly every vortex

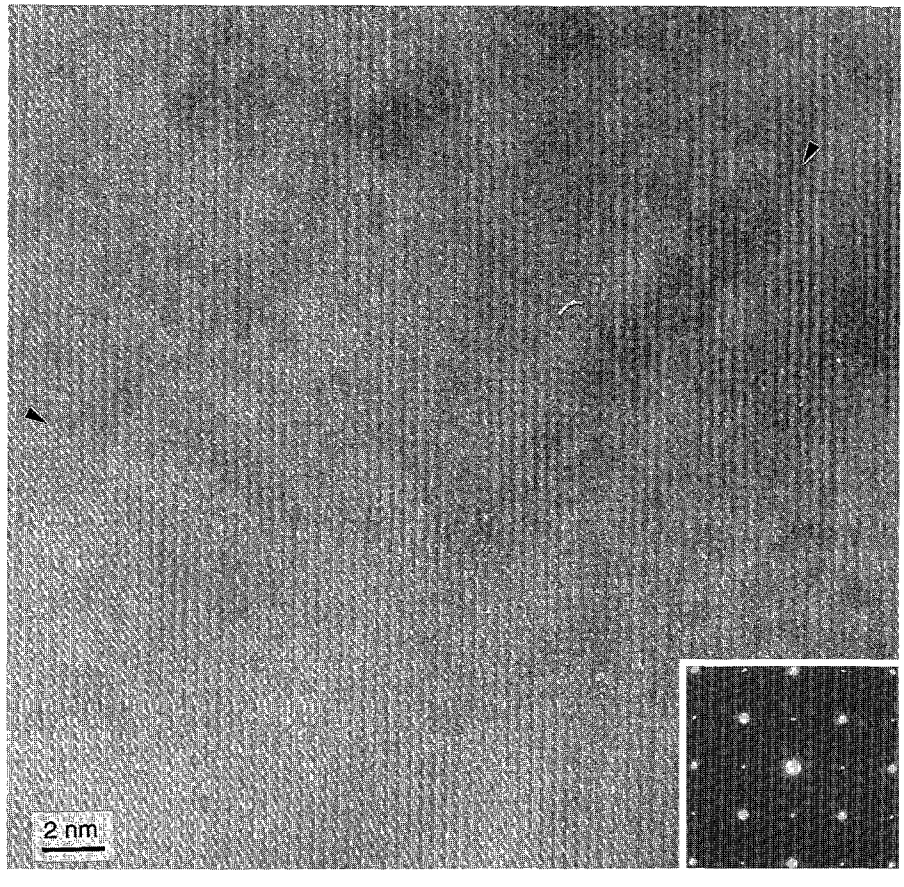

Fig. 10. A high-magnification [001] planar-view TEM image of YBCO showing planar boundaries in the grown film. The inset is an electron diffraction pattern recorded from this region.

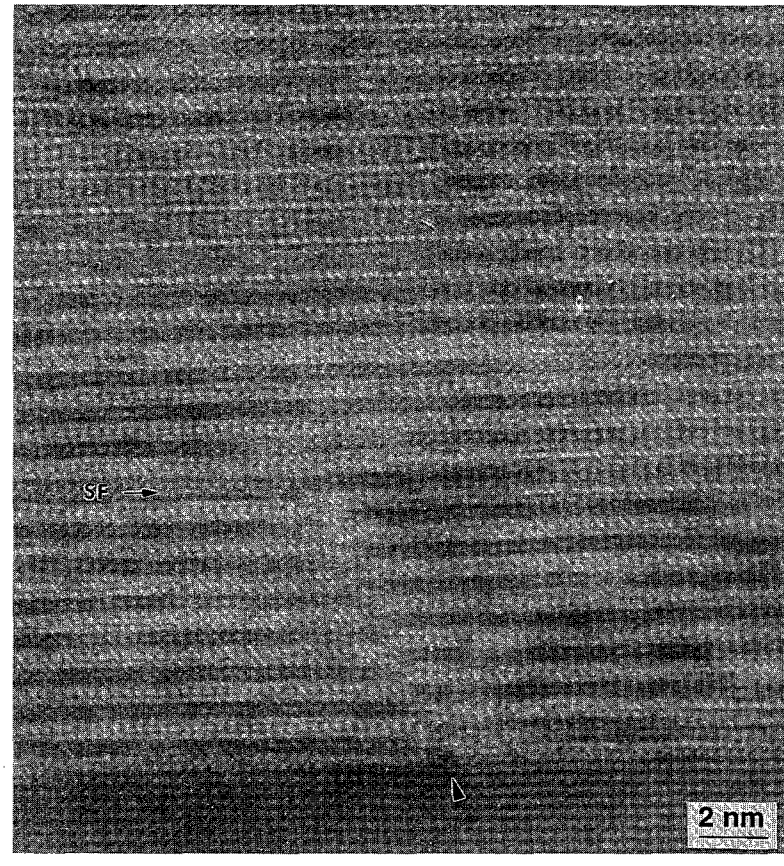

Fig. 11. A high-magnification [100] cross-section TEM image of YBCO showing the direct association of a defect with a substrate step/dislocation.

line when $H = 0.5$ T [5], but it is insufficient to pin all the vortices when the magnetic field is much stronger.

The density of substrate steps may not correspond directly with the density of the columnar defects. If the substrate step has an average height of 0.2 nm, the average distance between two adjacent steps is approximately 7 nm for a miscut angle of 1.6°. However, the average separation between the columnar defects is much larger than 7 nm, suggesting that the steps which provide nucleation sites for the columnar defects must be much higher than 0.2 nm. In addition, the growth for a columnar defect may be initiated from the sites of surface kinks, ledges, and dislocation edges, because there seems to be no reason for a columnar defect to be directly initiated from a straight step.

The TEM results are consistent with scanning tunneling microscopy observations of tilted-platelet microstructures [14], suggesting that the films might contain highly oriented internal growth defects, induced by the miscut-aligned growth. STM also revealed that the screw-mediated growth mechanism of YBCO films is suppressed in films grown on miscut substrates [2].

6. Conclusions

In conclusion, growth-induced columnar defects are formed in the YBCO films grown on deliberately miscut substrates. The columnar defects and small diameter stacking faults in the a–b-plane can produce useful amounts of flux pinning, particularly

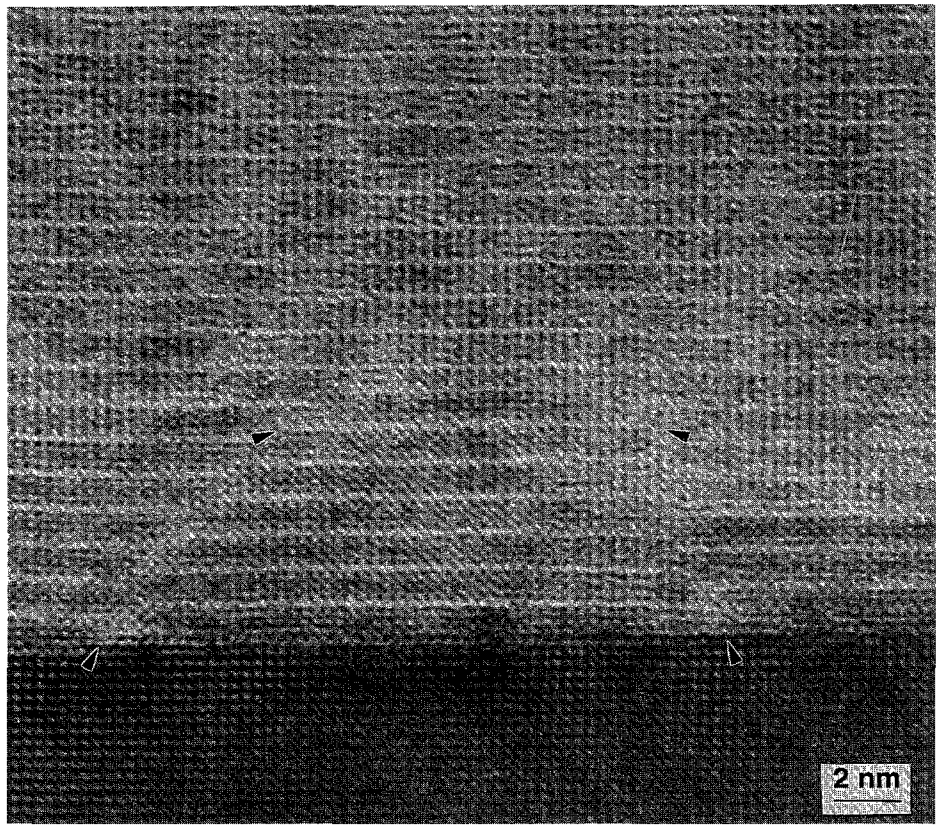

Fig. 12. A high-magnification [100] cross-section TEM image of YBCO showing defects initiated at the YBCO–substrate interface. In this case, the Cu–O planes broken by the defects are re-matched after the film is thicker than 10 nm.

when the applied field H is nearly parallel to the c-axis, resulting in an anomalous peak in J_c. The growth of columnar defects in the YBCO film is directly initiated at the steps/dislocations of the substrate surfaces, which are induced by the combination of substrate miscut and mosaic spread. Therefore, a proper control of the density of the columnar defects can optimize the critical current density when the magnetic field is between the c-axis and the a–b-plane of YBCO.

Acknowledgements

Research was supported in part by the US Department of Energy, Office of Advanced Utility Concepts – Superconducting Technology Program, under contract DE-AC05-84OR21400 with Lockheed Martin Energy Systems, Inc.

References

[1] R.K. Simon, C.E. Platt, K.P. Daly, A.E. Lee and M.K. Wagner, Appl. Phys. Lett. 53 (1988) 2677.
[2] D.H. Lowndes, X.Y. Zheng, S. Zhu, J.D. Budai and R.J. Warmack, Appl. Phys. Lett. 17 (1992) 852.
[3] S. Geller and V.B. Bala, Acta Crystallogr. 9 (1956) 1019.
[4] G.W. Berkstresser, A.J. Valentino and C.D. Brandle, J. Cryst. Growth 109 (1991) 467.
[5] D.H. Lowndes, D.K. Christen, C.E. Klabunde, Z.L. Wang, D.M. Kroeger, J.D. Budai, S. Zhu and D.P. Norton, Phys. Rev. Lett. 74 (1995) 2355.
[6] Z.L. Wang, D.K. Christen, C.E. Klabunde, D.M. Kroeger, D.H. Lowndes and D.P. Norton, in: Proc. 52nd Annual

Meeting of Microscopy Society of America, eds. G.W. Bailey and A.J. Garratt-Reed (San Francisco Press, New Orleans, 1994) p. 790.
[7] D.H. Lowndes, "Growth of Epitaxial Films by Pulsed-Laser Ablation," in: Modern Topics in Single Crystal Growth, eds. L.A. Boatner, K. Jackson and E. Bourret (American Institute of Physics, New York, 1995), to be published.
[8] Z.L. Wang, A. Goyal and D.M. Kroeger, Phys. Rev. B 47 (1993) 5373.
[9] D.K. Christen, J.R. Thompson, H.R. Kerchner, B.C. Sales, B.C. Chakoumakos, L. Civale, A.D. Marwick and F. Holtzberg, in: Superconductivity and Its Applications, Vol. 273, eds. H.S. Kwok, D.T. Shaw and M.J. Naughton (American Institute of Physics, New York, 1993) p. 24.
[10] Z.L. Wang, R. Kontra, A. Goyal and D.M. Kroeger, Materials Science Forum, 129 (1993) 1.
[11] Z.L. Wang and A.J. Shapiro, Surf. Sci. 328 (1995) 141; ibid, 328 (1995) 159.
[12] J.R. Thompson, Y.R. Sun, H.R. Kerchner, D.K. Christen, B.C. Sales, B.C. Chakoumakos, A.D. Marwick, L. Civale and J.O. Thomson, Appl. Phys. Lett. 60 (1992) 2306.
[13] L. Civale, A.D. Marwick, T.K. Worthington, M.A. Kirk, J.R. Thompson, L. Krusin-Elbaum, Y.R. Sun, J.R. Clem and F. Hotzberg, Phys. Rev. Lett. 67 (1991) 648.
[14] D.H. Lowndes, X.Y. Zheng, S. Zhu, J.D. Budai and R.J. Warmack, Appl. Phys. Lett. 17 (1992) 852.